THE JOURNAL OF PHYSICAL CHEMISTRY C

Article

pubs.acs.org/JPCC

Observation of Mixed Valence Ru Components in Zn Doped $Y_2Ru_2O_7$ Pyrochlores

G. Berti,[†] S. Sanna,[‡] C. Castellano,[§] J. Van Duijn,[∥] R. Ruiz-Bustos,[∥] L. Bordonali,[‡] G. Bussetti,[†] A. Calloni,[†] F. Demartin,[§] L. Duò,[†] and A. Brambilla*[,†]

[†]Dipartimento di Fisica, Politecnico di Milano, piazza Leonardo da Vinci 32, 20133 Milano, Italy

[‡]Dipartimento di Fisica and CNISM, Università di Pavia, viale Bassi 6, 27100 Pavia, Italy

[§]Dipartimento di Chimica, Università degli Studi di Milano, via Golgi 19, 20133 Milano, Italy

[∥]Departamento de Mecánica, Universidad de Córdoba, 14071 Córdoba, Spain

ABSTRACT: We present a study of $Y_{2-x}Zn_xRu_2O_7$ pyrochlores as a function of the Zn doping level x. X-ray diffraction measurements show that single-phase samples could be obtained for $x < 0.2$. Within the allowed range for x, dc conductivity measurements revealed a sizable decrease in resistivity at all the investigated temperatures for Zn doped samples with respect to undoped ones. Neutron diffraction data of the $x = 0.2$ sample showed that replacing Y^{3+} by Zn^{2+} does not result in the formation of oxygen vacancies. X-ray photoemission spectroscopy measurements revealed that part of the Ru ions are in the 5+ oxidation state to balance, in terms of electronic charge, the incorporation of Zn^{2+}. The results give experimental evidence that the heterovalent doping promotes the increase of conductivity in the $Y_2Ru_2O_7$ pyrochlores, making these systems promising as intermediate-temperature solid oxide fuel cell cathodes.

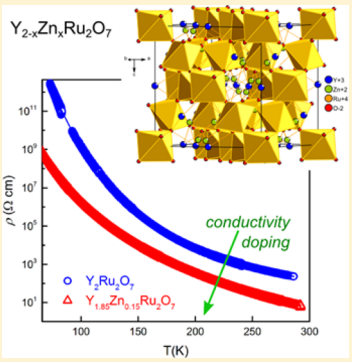

INTRODUCTION

In pyrochlore compounds, with general chemical formula $A_2B_2O_7$, both the A and B sites form an interpenetrating network of corner-sharing tetrahedra, resulting in a peculiar structure capable of exhibiting a spectacular number of fascinating physical properties.[1−3] Within this system, the family of ruthenium pyrochlores displays a multitude of interesting properties due to their high chemical and structural flexibility.[4−13] These properties include metal-insulator, long-range order, and spin-singlet transitions. Moreover, very good electrochemical behavior of Ru based pyrochlores has been observed at temperatures as low as 350 °C, which has motivated their study as intermediate-temperature solid oxide fuel cell (IT-SOFC) cathodes.[14−17]

The wide variety of ground states observed is due to the fact that Ru can be either in the 4+ or 5+ oxidation state, promoting good electrical and catalytic properties.[6,18] While the majority of the work has been done on materials in which the A site is fully occupied by either 3+ (Ru^{4+}) or 2+ (Ru^{5+}) cations, there are few studies reporting the effect of having a mixed oxidation state on the A site.[1,2] Doping the A sites with 2+ cations could result in a hole doping effect concomitant with an increased concentration of disordered oxygen vacancies in these oxides;[19−23] this is expected to provide them with the required ionic conductivity to be used as cathodes in IT-SOFC.[24−29]

In this work, we present a study of the physical properties of $Y_{2-x}Zn_xRu_2O_7$ (Zn^{2+} doped system).[30] Due to the importance of clarifying in detail the effect of this type of doping on the cationic and anionic stoichiometry (and on the related structural features), we used a set of complementary techniques. X-ray powder diffraction (XRD) was employed to provide information on the crystallographic structure and phase purity of the samples. DC transport measurements were carried out in order to assess the influence of the Zn doping on the electrical conductivity of the specimens. Neutron powder diffraction (NPD) was used to study possible deviations in oxygen stoichiometry and possible structural changes, on account of the contrast between the scattering lengths of the different elements (i.e., NPD is more sensitive to lighter elements compared to XRD). Finally, X-ray photoemission spectroscopy (XPS) was exploited to determine, in particular, the valence state of the elements.

Our measurements show that single-phase samples of $Y_{2-x}Zn_xRu_2O_7$ could be obtained up to a doping level of $x < 0.2$. Unlike what one would expect, the substitution of Y^{3+} by Zn^{2+} does not result in the formation of oxygen vacancies. Instead, Ru atoms become mixed valent (4+/5+). As a result, the resistivity of the doped samples is significantly reduced compared to undoped $Y_2Ru_2O_7$.

EXPERIMENTAL METHODS

Powdered samples of $Y_{2-x}Zn_xRu_2O_7$ ($x = 0$, $x = 0.1$, $x = 0.15$, $x = 0.2$, $x = 0.3$, and $x = 0.5$) were synthesized using the solid state reaction method. Mixtures of Y_2O_3, ZnO, and RuO_2 in

Received: December 18, 2015
Revised: May 13, 2016

DOI: 10.1021/acs.jpcc.5b12411
J. Phys. Chem. C XXXX, XXX, XXX−XXX

proper molar ratios were intimately mixed by ball milling for 2 h at 250 rpm, pressed into pellets, and reacted at 1000−1200 °C for 24 h in air with intermediate grindings. For the neutron diffraction experiment, 3 g of $Y_{1.8}Zn_{0.2}Ru_2O_7$ was prepared by ball milling the starting reactants (weighed in proper molar ratio) for 3 h at 200 rpm, pressing them into pellets, and sintering at 1200 °C in air for 24 h with one intermediate grinding. All samples were characterized by X-ray diffraction (XRD) using a Philips XPert Pro diffractometer with a copper source and incident beam monochromator and by scanning electron microscopy (SEM) using a JEOL JSM 5500 LV equipped with an IXRF EDS 2000 backscatter detector (BSE, 20 kV excitation voltage, 10 pA beam current, 2 mm beam diameter).

Room temperature NPD data were collected on 3 g of $Y_{0.8}Zn_{0.2}Ru_2O_7$ using the General Materials (GEM) Diffractometer at the ISIS Facility, Rutherford Appleton Laboratory, U.K., via the GEM Xpress service. Rietveld analyses of the X-ray and neutron powder diffraction patterns were performed by means of the Fullprof suite and GSAS software packages.[31,32]

The electrical resistivity was measured using a HP 34401A Multimeter in the standard dc four probe modality. The measurements were carried out as a function of temperature in the range 80−300 K on pellets with dimensions 2 × 2 × 13 mm^3, sintered at 1100 °C for 24 h. Due to the low conducting ceramic character of the samples, the electrical contacts were improved by sputtering a spot of Pd metal for each contact on the surface.

XPS measurements were performed at room temperature in a ultrahigh vacuum system (base pressure $<5 \times 10^{-8}$ Pa)[33] on powder firmly stuck onto an In foil. Spectra were acquired with a SPECS Phoibos 150 mm hemispherical electron analyzer operated at a fixed pass energy of 20 eV. Electrons were excited with Mg Kα radiation ($h\nu$ = 1253.6 eV). The overall resolution was of about 1 eV. Satellites from the X-ray source were subtracted from the experimental data. The XPS line shape analysis, in terms of peak fitting and spectra deconvolution, was based on symmetric profiles made up of a product of Gaussian and Lorentzian line shapes, summed to an integral (Shirley) background.[34,35]

Finally, in order to ascertain the homogeneity of the prepared samples and to verify that the bulk composition is the same as that of the surface, we have performed X-ray fluorescence (XRF) by using a Panalytical Epsilon 1 spectrometer, equipped with a thin-window Ag anode X-ray tube, operating between 10 and 50 kV. For each compound, by selective sieving after grinding, samples having different crystallite sizes were analyzed. In this way it was possible to guarantee that the obtained analytical results were representative of the entire bulk and not of the sample surface only.

RESULTS AND DISCUSSION

To determine the limit at which Zn can substitute Y in $Y_2Ru_2O_7$, we carried out XRD measurements on all prepared samples. The results are shown in Figure 1a). In all profiles, the cubic pyrochlore structure is observed as the main phase. The expanded view presented in the inset, however, reveals that for x = 0.2 we start to observe unreacted ZnO. This suggests that the maximum solubility limit, under ambient conditions, of Zn into $Y_2Ru_2O_7$ is just less than 10 atom %. This is lower than what is observed for other reported substitutions by 2+ ions; e.g., in the case of Ca the substitution limit appears to be 30%.[1]

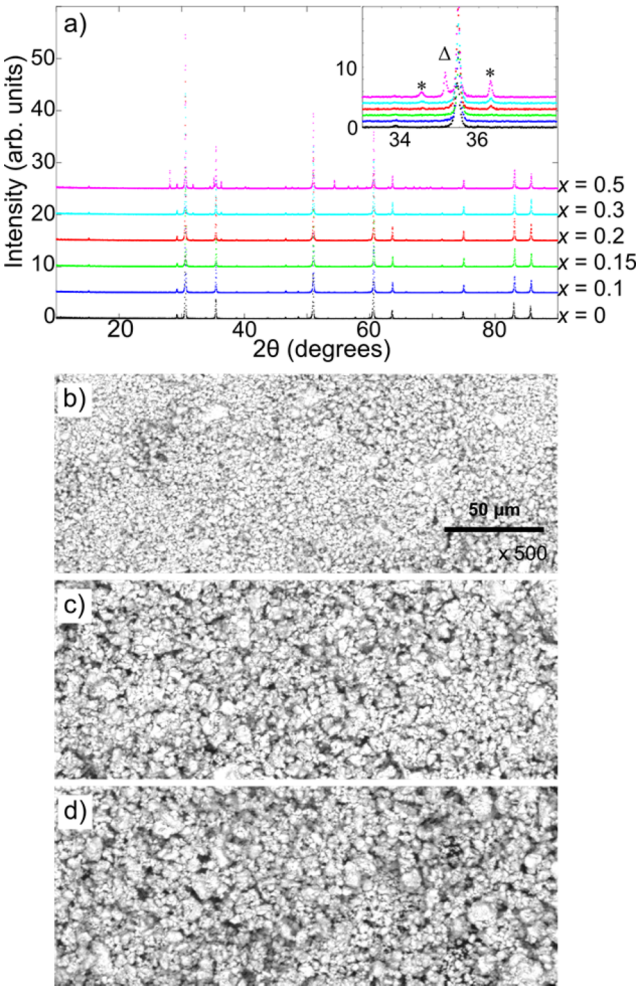

Figure 1. (a) X-ray powder diffraction profiles of $Y_{2-x}Zn_xRu_2O_7$, for x in the range from 0 to 0.5. The inset shows part of the diffraction profile revealing the presence of unreacted ZnO (∗) for $x \geq 0.2$. A peak due to unreacted Y_2O_3 is indicated by Δ. For the sake of clarity, the diffraction profiles have been vertically offset from each other. (b) SEM-BSE images of $Y_{2-x}Zn_xRu_2O_7$ for x = 0. (c and d) Same images for x = 0.1 and x = 0.15, respectively. The scale is the same for all images.

On the other hand, in the case of Ca, 100% substitution can be obtained using high pressure synthesis methods.[36]

SEM-BSE images are shown in Figure 1b−d for the x = 0, x = 0.10, and x = 0.15 compositions. Such images show neither inhomogeneities nor spurious phases, therefore confirming that the low-doped samples are pure in phase. Concerning the XRF analysis, all the values of chemical composition obtained for the various portions of each sample, as described under Experimental Methods, were identical within one estimated standard deviation. As far as the zinc content is concerned, we have obtained compositions, expressed in terms of ZnO wt %, that were consistent with the respective theoretical values. In particular, the ZnO content was in the ranges 3.28(7)−3.37(7) for $Y_{1.80}Zn_{0.20}Ru_2O_7$ (expected value 3.34 wt %), 2.47(8)−2.54(8) for $Y_{1.85}Zn_{0.15}Ru_2O_7$ (expected value 2.50 wt %), and 1.57(9)−1.60(9) for $Y_{1.90}Zn_{0.10}Ru_2O_7$ (expected value 1.66 wt %).

Table 1 summarizes the effect that the substitution of Y by Zn has on the lattice parameter of $Y_{2-x}Zn_xRu_2O_7$, as obtained from Rietveld fits of the XRD profiles shown in Figure 1. From

DOI: 10.1021/acs.jpcc.5b12411
J. Phys. Chem. C XXXX, XXX, XXX−XXX

Table 1. Lattice Parameter Dependence of $Y_{2-x}Zn_xRu_2O_7$ due to Substitution of Y by Zn[a]

doping level, x	lattice param (Å)	χ^2	R_{Bragg} (%)	R_f (%)
0.00	10.1427(5)	1.54	23.4	15.8
0.10	10.1296(5)	1.75	27.7	16.5
0.15	10.1295(5)	2.46	10.9	12.3
0.20	10.1302(5)	3.18	7.44	10.3
0.30	10.1283(5)	3.12	8.5	10.5
0.50	10.1278(5)	7.13	11.0	15.1

[a]The values of the lattice parameter as a function of x were obtained by Rietveld analysis of the diffraction profiles shown in Figure 1. The goodness of fit parameters are reported: R_f, R_{Bragg}, and χ^2 are R (agreement) and goodness of fit parameters, respectively.

Table 1 we can see that, as the Zn content increases up to about x = 0.10−0.15, the lattice parameter decreases. This reduction is due to the fact that the ionic radius of Zn^{2+} is smaller than that of Y^{3+}.[37] For x > 0.15, on the other hand, no significant change to the lattice parameter is observed. This is consistent with the observation of unreacted ZnO in the X-ray diffraction patterns shown in Figure 1, confirming that the solubility limit of Zn into $Y_2Ru_2O_7$ is less than 10%.

In Figure 2 dc transport measurements are displayed for x = 0 and x = 0.15. The data related to the undoped sample can be

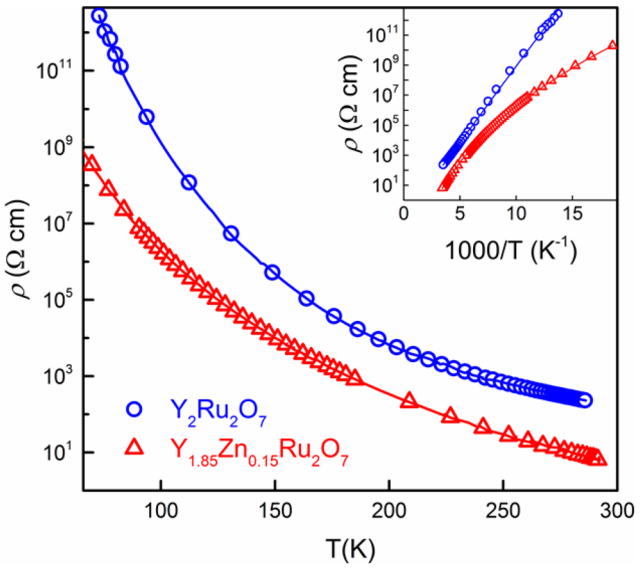

Figure 2. Temperature dependence of the electric resistivity of $Y_{2-x}Zn_xRu_2O_7$ for x = 0 (circles) and x = 0.15 (triangles). The inset shows the same data in the semilogarithmic scale as a function of inverse temperature. The continuous lines are guides to the eye.

nicely fitted by a Arrhenius-type law, $\rho = \rho_0 \exp(E_a/k_BT)$ (blue line in the inset of Figure 2) with an activation energy of the hopping conduction of the localized holes, E_a = 0.19(1) eV. This is in agreement with the Mott−Hubbard insulating behavior previously observed for $Y_2Ru_2O_7$.[38] The nonlinear behavior displayed in the inset for x = 0.15 indicates that the Zn doped sample does not follow a simple Arrhenius-type law. A detailed study of its temperature dependence is beyond the scope of this work. Notably, for the Zn doped sample the electric resistivity is reduced by about a factor 10^2 at room temperature and even more at low temperature. This gives clear evidence that the heterovalent Y^{3+} by Zn^{2+} substitution makes the system significantly more metallic. These changes of the electric properties can be due to either Ru becoming mixed valent ($Y_{2-x}Zn_xRu^{4+}{}_{2-x}Ru^{5+}{}_xO_7$) or Ru staying 4+ valent while the system creates oxygen vacancies ($Y_{2-x}Zn_xRu^{4+}{}_2O_{7-x/2}$) to charge compensate substitution.

With the aim of establishing which is the correct scenario, we performed an NPD study on $Y_{1.8}Zn_{0.2}Ru_2O_7$ (Figure 3). Careful

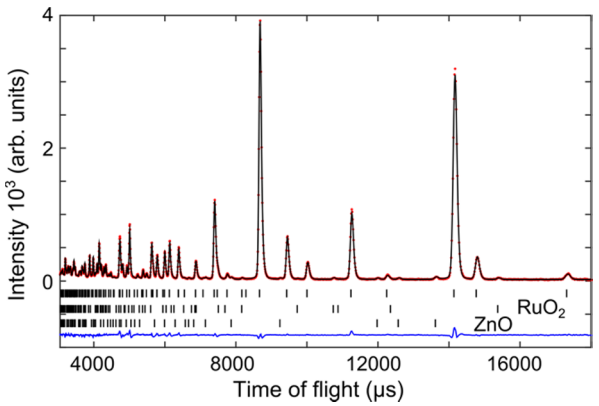

Figure 3. Neutron powder diffraction (NPD) pattern of $Y_{1.8}Zn_{0.2}Ru_2O_7$ from the GEM 63.62° 2θ detector bank, collected at room temperature. The solid black line shows the Rietveld fit to the data; the residual of the fit (blue line) is shown at the bottom of the plot. The upper, middle, and lower tick marks indicate Bragg reflections coming from the crystal structure of either $Y_{1.8}Zn_{0.2}Ru_2O_7$ or the RuO_2 and ZnO impurity phases, respectively.

analysis of the data revealed that the sample adopts the cubic pyrochlore, and that it contains 0.8(1) and 1.0(1) mass % of unreacted RuO_2 and ZnO, respectively. No evidence was found of any long-range structural change when substituting Y by Zn. Allowing the relative Y/Zn occupancy to vary (but fixing the overall occupancy for the A site to 1) showed that the amount of Y substituted by Zn in this sample, x = 0.22(2), is very close to the theoretical value x = 0.2.

In order to determine whether the substitution of Y^{3+} by Zn^{2+} gets charge compensated by the formation of O^{2-} vacancies, we tried to refine the occupancies of the O sites. In all three cases (refining the occupancy of either only O(1) or only O(2) or both O sites) the occupancy of the O sites was refined (within experimental error) to 1. Therefore, from our NPD study we find no evidence for the formation of oxygen vacancies within the material, suggesting that Ru should be mixed valent. The results of the best fit to the data (fixing the O occupancies to 1 and allowing the Y/Zn occupancy of the A site to vary) are shown in Figure 3 and Table 2. We notice that the difference between the lattice parameters derived from either XRD (Table 1) or NPD (Table 2) is much likely due to the better experimental resolution of the latter technique.

In order to check for the presence of mixed valence Ru states, the effects of Zn doping on the electronic states of Ru were investigated by means of XPS. In particular, mixed valence would correspond to the occurrence of multiple peaks in core level features, originated by the chemical shift that would occur on account of the different charge transfer.[39,40] Figure 4a shows a wide XPS scan of the $Y_2Ru_2O_7$ sample, covering the binding energy region from the Fermi level down to about 1000 eV. In such an overview scan, the main contributions coming from Y, Ru, and O core levels are evidenced by the peak labels. In particular, the spectrum features a contribution also from the C 1s core level, due to the presence of contaminants on the

DOI: 10.1021/acs.jpcc.5b12411
J. Phys. Chem. C XXXX, XXX, XXX−XXX

Table 2. Structural Parameters of the Best Fit to the Neutron Powder Diffraction Pattern of $Y_{1.8}Zn_{0.2}Ru_2O_7$[a]

atom	site	x	y	z	B (Å^2)	occupancy
Y	16d	1/2	1/2	1/2	0.49(1)	0.89(1)
Zn	16d	1/2	1/2	1/2	0.49(1)	0.11(1)
Ru	16c	0	0	0	0.14(1)	1
O(1)	48f	0.33438(6)	1/8	1/8	0.45(1)	1
O(2)	8b	3/8	3/8	3/8	0.47(2)	1
a = 10.1141(1) Å			global χ^2 = 4.59			
63.62° 2θ detector bank:			R_{Bragg} = 2.87%		R_f = 3.18%	
91.3° 2θ detector bank:			R_{Bragg} = 2.74%		R_f = 5.00%	
154.4° 2θ detector bank:			R_{Bragg} = 4.20%		R_f = 4.62%	

[a]The parameters were collected in the 63.62, 91.3, and 154.4° 2θ detector banks at room temperature on GEM. B is the isotropic thermal factor. R_f, R_{Bragg}, and χ^2 are R (agreement) and goodness of fit parameters, respectively. The crystal structure is cubic with space group $Fd\bar{3}m$.

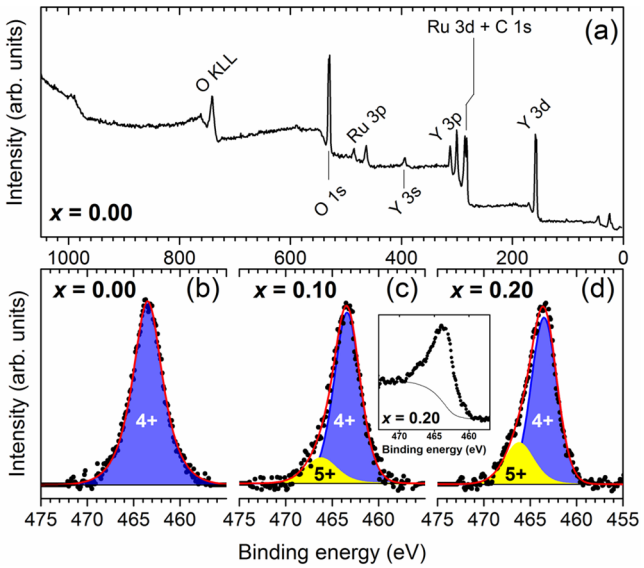

Figure 4. (a) XPS wide spectrum of the $Y_2Ru_2O_7$ sample. The contributions from the different core levels are evidenced by the peak labels. Bottom row: background-subtracted XPS spectra of Ru $3p_{3/2}$ peaks, for x = 0 (b), x = 0.1 (c), and x = 0.2 (d). Fittings of the peaks in panels from (b) to (d) are given in blue (Ru^{4+}) and yellow (Ru^{5+}), while background-subtracted data are shown as dots. The red solid line is the sum of the two fitting contributions. The inset reports the as-collected XPS spectrum of Ru $3p_{3/2}$ peaks, for x = 0.2, together with the relative integral background, before subtraction.

surface (typically airborne components). Since such a core level superimposes to the Ru 3d states, the following analysis was carried out by inspecting the line shape of the Ru 3p states.

Figure 4b–d shows, in particular, the Ru $3p_{3/2}$ XPS peaks (circles) for samples characterized by x = 0, x = 0.1, and x = 0.2. The shadowed profiles represent instead spectral deconvolutions of the XPS peaks, based on symmetric profiles (see Experimental Methods). Both spectra and their deconvolutions are represented after the subtraction of an integral background. When inspecting the spectral line shapes and the corresponding deconvolutions, it was seen that the peak relative to the undoped sample (Figure 4b) could be fitted by a single contribution at a binding energy (BE) of 463.4(3) eV, which is well within the range of 4+ valence state for Ru.[41−44] On the other hand, the measured peaks relative to the doped samples (Figure 4c,d) could not be fitted by a single contribution. The hypothetical possibility of having mixed valent Ru would correspond to the detection, in the spectra, of the presence of a contribution from Ru atoms in the 5+ valence state. Such a contribution would be located at a slightly higher binding energy with respect to that associated with Ru^{4+} species. References to the value of such a chemical shift are very scarce in the literature, so a prediction of the energy position for a secondary peak is difficult. On the other hand, fitting the XPS spectra of the doped samples with two contributions was indeed possible. The first contribution (shaded in blue) is located at the same binding energy as the undoped one and can therefore be associated with Ru in the 4+ valence state. The second one (shaded in yellow) is located at 465.9(3) eV and can be ascribed to Ru^{5+}.

The peak associated with Ru^{5+} species appears only when substituting Y with Zn. From the relative intensities of such peaks it is also possible to perform a quantitative analysis and estimate the relative amount of Ru atoms in the 5+ valence state. The intensity of each peak was calculated as the integral of the subtended area; this was then normalized by a proper relative sensitivity factor, on account of the different photoemission cross section for each element.

In the case of perfect stoichiometry, one would expect the $Ru^{5+}/(Ru^{5+} + Ru^{4+})$ intensity ratio to be equal to x. Even if our analysis is hindered by the relatively low intensity of the signals, the results confirm a good agreement between the nominal Zn stoichiometry and the estimated fraction of Ru^{5+}. The XPS results give therefore clear experimental evidence that each Zn/Y substitution induces a hole yielding a mixed valent Ru^{5+} + Ru^{4+} state. This process is responsible for the sizable increase of the conductivity of the $Y_{2-x}Zn_xRu_2O_7$ for x = 0.15 with respect to the undoped one, as shown in Figure 2.

CONCLUSIONS

In summary, we presented an electrical, chemical, and structural characterization of Zn doped $Y_{2-x}Zn_xRu_2O_7$ pyrochlores, giving evidence of successful Y substitution for x < 0.2 and of an increase in electric conductivity after doping.

While neutron diffraction data suggest that no oxygen vacancies form as a consequence of doping, X-ray photoemission spectroscopy data reveal that a fraction of Ru atoms, fairly corresponding to the nominal doping level, acquires the 5+ valence state in the doped compounds. Ru in Zn doped $Y_{2-x}Zn_xRu_2O_7$ pyrochlores is therefore in a mixed valent Ru^{5+}+Ru^{4+} state. These results encourage further studies of doped pyrochlores as intermediate-temperature solid oxide fuel cell cathodes.

AUTHOR INFORMATION

Corresponding Author

*E-mail: alberto.brambilla@polimi.it. Tel.: +390223996170.

Present Address

L.B.: IMT—Institute of Microstructure Technology, Karlsruhe Institute of Technology, Hermann von-Helmholtz Platz 1, 76344 Eggenstein-Leopoldshafen, Germany.

Notes

The authors declare no competing financial interest.

ACKNOWLEDGMENTS

This work was partially supported by the Ramón y Cajal program through Grant RYC-2005-001064, the Ministerio de

DOI: 10.1021/acs.jpcc.5b12411
J. Phys. Chem. C XXXX, XXX, XXX−XXX

Ciencia y Tecnología through Grant MAT2010-15245, and the Consejería de Educación y Ciencia of the Junta de Comunidades de Castilla-La Mancha through Grant PII1I09-0083-2105. We would also like to thank the Science and Technology Facilities Council (STFC) for providing us with Xpress beamtime on GEM. J.V.D. would like to thank Prof. Glenn Kowach for his fruitful discussions on analyzing the NPD data. C.C. would like to thank Italo Campostrini for SEM image acquisition. M. C. Mozzati and P. Carretta are gratefully acknowledged for helpful discussions. The research of A.C. is funded by Fondazione Cariplo (2013 SHAPES project, Grant 2013-0736).

REFERENCES

(1) Subramanian, M. A.; Aravamudan, G.; Subba Rao, G. V. Oxide Pyrochlores — A Review. *Prog. Solid State Chem.* **1983**, *15*, 55−143.
(2) Weller, M. T.; Hughes, R. W.; Rooke, J.; Knee, C. S.; Reading, J. The Pyrochlore Family − a Potential Panacea For the Frustrated Perovskite Chemist. *Dalton Trans.* **2004**, *19*, 3032−3041.
(3) Gardner, J. S.; Gingras, M. J. P.; Greedan, J. E. Magnetic Pyrochlore Oxides. *Rev. Mod. Phys.* **2010**, *82*, 53−107.
(4) Yoshii, S.; Sato, M. Studies on Metal-Insulator Transition of Pyrochlore Compound $Y_{2-x}Bi_xRu_2O_7$. *J. Phys. Soc. Jpn.* **1999**, *68*, 3034−3040.
(5) Haas, M. K.; Cava, R. J.; Avdeev, M.; Jorgensen, J. D. Robust Paramagnetism in $Bi_{2-x}M_xRu_2O_7$ (M = Mn,Fe,Co,Ni,Cu) Pyrochlore. *Phys. Rev. B: Condens. Matter Mater. Phys.* **2002**, *66*, 094429.
(6) Sathiya, M.; Ramesha, K.; Rousse, G.; Foix, D.; Gonbeau, D.; Prakash, A. S.; Doublet, M. L.; Hemalatha, K.; Tarascon, J.-M. High Performance $Li_2Ru_{1-y}Mn_yO_3$ ($0.2 \leq y \leq 0.8$) Cathode Materials for Rechargeable Lithium-Ion Batteries: Their Understanding. *Chem. Mater.* **2013**, *25*, 1121−1131.
(7) Wang, R.; Sleight, A. W. Synthesis and Characterization of $Cd_2Ru_2O_7$. *Mater. Res. Bull.* **1998**, *33*, 1005−1007.
(8) Li, L.; Kennedy, B. J. Structural and Electronic Properties of the Ru Pyrochlores $Bi_{2-y}Yb_yRu_2O_{7-\delta}$. *Chem. Mater.* **2003**, *15* (21), 4060−4067.
(9) Yamamoto, A.; Sharma, P. A.; Okamoto, Y.; Nakao, A.; Katori, H. A.; Niitaka, S.; Hashizume, D.; Takagi, H. Metal−Insulator Transition in a Pyrochlore-type Ruthenium Oxide, $Hg_2Ru_2O_7$. *J. Phys. Soc. Jpn.* **2007**, *76*, 043703.
(10) Castellano, C.; Ferretti, M.; Martinelli, A.; Cimberle, M. R. Structural and Magnetic Properties of Cu Substituted Manganites Studied by EXAFS and DC Magnetization Measurements. *J. Alloys Compd.* **2009**, *478*, 479−483.
(11) Zhang, Z.; Middleburgh, S. C.; de los Reyes, M.; Lumpkin, G. R.; Kennedy, B. J.; Blanchard, P. E. R.; Reynolds, E.; Jang, L.-Y. Gradual Structural Evolution from Pyrochlore to Defect-Fluorite in $Y_2Sn_{2-x}Zr_xO_7$: Average vs Local Structure. *J. Phys. Chem. C* **2013**, *117*, 26740−26749.
(12) Atuchin, V. V.; Molokeev, M. S.; Yurkin, G. Yu.; Gavrilova, T. A.; Kesler, V. G.; Laptash, N. M.; Flerov, I. N.; Patrin, G. S. Synthesis, Structural, Magnetic, and Electronic Properties of Cubic $CsMnMoO_3F_3$ Oxyfluoride. *J. Phys. Chem. C* **2012**, *116*, 10162−10170.
(13) Castellano, C.; Berti, G.; Sanna, S.; Ruiz-Bustos, R.; Van Duijn, J.; Brambilla, A.; Muñoz-Noval, Á.; Carretta, P.; Duò, L.; Demartin, F. Evidence of Local Structural Order and Spin-Lattice Coupling in the Frustrated Pyrochlore $Y_2Ru_2O_7$. *Phys. Rev. B: Condens. Matter Mater. Phys.* **2015**, *91*, 224101.
(14) Goodenough, J. B.; Manoharan, R.; Paranthaman, P. Surface Protonation and Electrochemical Activity of Oxides In Aqueous Solution. *J. Am. Chem. Soc.* **1990**, *112*, 2076−2082.
(15) Bae, J.-M.; Steele, B. C. H. Properties of Pyrochlore Ruthenate Cathodes for Intermediate Temperature Solid Oxide Fuel Cells. *J. Electroceram.* **1999**, *3*, 37−46.
(16) Ehora, G.; Daviero-Minaud, S.; Steil, M. C.; Gengembre, L.; Frère, M.; Bellayer, S.; Mentré, O. Ru-Pyrochlores: Compositional Tuning for Electrochemical Stability as Cathode Materials for IT-SOFCs. *Chem. Mater.* **2008**, *20*, 7425−7433.
(17) Abate, C.; Esposito, V.; Duncan, K.; Nino, J. C.; Gattia, D. M.; Wachsman, E. D.; Traversa, E. Novel $Y_{2-x}Pr_xRu_2O_7$ (x = 0−2) Pyrochlore Oxides Prepared Using a Soft Chemistry Route and their Electrical Properties. *J. Am. Ceram. Soc.* **2010**, *93*, 1970−1977.
(18) Sardar, K.; Petrucco, E.; Hiley, C. I.; Sharman, J. D. B.; Wells, P. P.; Russell, A. E.; Kashtiban, R. J.; Sloan, J.; Walton, R. I. Water-Splitting Electrocatalysis in Acid Conditions Using Ruthenate-Iridate Pyrochlores. *Angew. Chem., Int. Ed.* **2014**, *53* (41), 10960−10964.
(19) Pirzada, M.; Grimes, R. W.; Maguire, J. F. Incorporation Of Divalent Ions in $A_2B_2O_7$ Pyrochlores. *Solid State Ionics* **2003**, *161*, 81−91.
(20) Kramer, S.; Spears, M.; Tuller, H. L. Conduction in Titanate Pyrochlores: Role of Dopants. *Solid State Ionics* **1994**, *72*, 59−66.
(21) Gill, J. K.; Pandey, O. P.; Singh, K. Ionic Conductivity, Structural and Thermal Properties of Ca^{2+} Doped $Y_2Ti_2O_7$ Pyrochlores for SOFC. *Int. J. Hydrogen Energy* **2012**, *37*, 3857−3864.
(22) Kim, N.; Grey, C. P. Solid-state NMR Study of the Anionic Conductor Ca-Doped $Y_2Ti_2O_7$. *Dalton Trans.* **2004**, *19*, 3048−3052.
(23) Yoshii, S.; Murata, K.; Sato, M. Metal-insulator Transition of $R_{2-x}Ca_xRu_2O_7$ (R = Y, Sm). *J. Phys. Chem. Solids* **2001**, *62*, 129−134.
(24) Sagarna, L.; Populoh, S.; Shkabko, A.; Eilertsen, J.; Maegli, A. E.; Hauert, R.; Schrade, M.; Karvonen, L.; Weidenkaff, A. Influence of the Oxygen Content on the Electronic Transport Properties of $Sr_xEu_{1-x}TiO_{3-\delta}$. *J. Phys. Chem. C* **2014**, *118*, 7821−7831.
(25) Reddy, B. M.; Bharali, P.; Saikia, P.; Park, S.-E.; Van Den Berg, M. W. E.; Muhler, M.; Grünert, W. Structural Characterization and Catalytic Activity of Nanosized $Ce_xM_{1-x}O_2$ (M = Zr and Hf) Mixed Oxides. *J. Phys. Chem. C* **2008**, *112*, 11729−11737.
(26) Jaiswal, A.; Wachsman, E. D. Impedance studies on Bismuth-Ruthenate-Based Electrodes. *Ionics* **2009**, *15*, 1−9.
(27) Martínez-Coronado, R.; Aguadero, A.; de la Calle, C.; Fernandez, M. T.; Alonso, J. A. Evaluation of the R_2RuMnO_7 Pyrochlores as Cathodes in Solid-Oxide Fuel Cells. *J. Power Sources* **2011**, *196*, 4181−4186.
(28) Martínez-Coronado, R.; Alonso, J. A.; Cascos, V.; Fernández-Díaz, M. T. Crystal and Magnetic Structure of the Bi_2RuMnO_7 Pyrochlore: A Potential New Cathode for Solid Oxide Fuel Cells. *J. Power Sources* **2014**, *247*, 876−882.
(29) Modeshia, D. R.; Wright, C. S.; Payne, J. L.; Sankar, G.; Fiddy, S. G.; Walton, R. I. Low-Temperature Redox Properties of Nanocrystalline Cerium (IV) Oxides Revealed by in Situ XANES. *J. Phys. Chem. C* **2007**, *111*, 14035−14039.
(30) Berti, G.; Sanna, S.; Ruiz-Bustos, R.; van Duijn, J.; Brambilla, A.; Muñoz-Noval, Á.; Demartin, F.; Duò, L.; Castellano, C. Evidence of a Correlation between Magnetic and Structural Transitions in $Y_{2-x}Zn_xRu_2O_7$ Pyrochlore Compounds. *RSC Adv.* **2015**, *5*, 100809−100815.
(31) Rodriguez-Carvajal, J. Recent Advances in Magnetic Structure Determination by Neutron Powder Diffraction. *Phys. B* **1993**, *192*, 55−69.
(32) Larson, A. C.; Dreel, R. B. V. *General Structure Analysis System (GSAS)*; Los Alamos National Laboratory Report LAUR 86-748; 2000.
(33) Berti, G.; Calloni, A.; Brambilla, A.; Bussetti, G.; Duò, L.; Ciccacci, F. Direct Observation of Spin-Resolved Full And Empty Electron States In Ferromagnetic Surfaces. *Rev. Sci. Instrum.* **2014**, *85*, 073901.
(34) Fairley, N. Casa Software Ltd. http://www.casaxps.com/.
(35) Evans, S. Curve Synthesis and Optimization Procedures for X-ray Photoelectron Spectroscopy. *Surf. Interface Anal.* **1991**, *17*, 85−93.
(36) Munenaka, T.; Sato, H. A Novel Pyrochlore Ruthenate: $Ca_2Ru_2O_7$. *J. Phys. Soc. Jpn.* **2006**, *75*, 103801−103804.
(37) Shannon, R. D. Revised Effective Ionic Radii and Systematic Studies of Interatomic Distances in Halides and Chalcogenides. *Acta Crystallogr., Sect. A: Cryst. Phys., Diffr., Theor. Gen. Crystallogr.* **1976**, *A32*, 751−767.

DOI: 10.1021/acs.jpcc.5b12411
J. Phys. Chem. C XXXX, XXX, XXX−XXX

(38) Yasukawa, M.; Kuniyoshi, S.; Kono, T. Thermoelectric Properties of the $Bi_{2-x}Y_xRu_2O_7$ (x = 0−2) Pyrochlores. *Solid State Commun.* **2003**, *126*, 213−216.
(39) Brambilla, A.; Calloni, A.; Berti, G.; Bussetti, G.; Duò, L.; Ciccacci, F. Growth and Interface Reactivity of Titanium Oxide Thin Films on Fe(001). *J. Phys. Chem. C* **2013**, *117*, 9229−9236.
(40) Calloni, A.; Brambilla, A.; Berti, G.; Bussetti, G.; Canesi, E. V.; Binda, M.; Petrozza, A.; Finazzi, M.; Ciccacci, F.; Duò, L. X-ray Photoemission Spectroscopy Investigation of the Interaction between 4-Mercaptopyridine and the Anatase TiO_2 Surface. *Langmuir* **2013**, *29*, 8302−8310.
(41) Ernst, M.; Sloof, W. Unraveling the Oxidation of Ru Using XPS. *Surf. Interface Anal.* **2008**, *40*, 334−337.
(42) Kim, H.-D.; Noh, H.-J.; Kim, K. H.; Oh, S.-J. Core-Level X-Ray Photoemission Satellites in Ruthenates: A New Mechanism Revealing The Mott Transition. *Phys. Rev. Lett.* **2004**, *93*, 126404.
(43) Kodintsev, I. M.; Trasatti, S.; Rubel, M.; Wieckowski, A.; Kaufher, N. X-ray Photoelectron Spectroscopy and Electrochemical Surface Characterization of Iridium(IV) Oxide + Ruthenium(IV) Oxide Electrodes. *Langmuir* **1992**, *8*, 283−290.
(44) Qadir, K.; Joo, S. H.; Mun, B. S.; Butcher, D. R.; Renzas, J. R.; Aksoy, F.; Liu, Z.; Somorjai, G. A.; Park, J. Y. Intrinsic Relation between Catalytic Activity of CO Oxidation on Ru Nanoparticles and Ru Oxides Uncovered with Ambient Pressure XPS. *Nano Lett.* **2012**, *12*, 5761−5768.

DOI: 10.1021/acs.jpcc.5b12411
J. Phys. Chem. C XXXX, XXX, XXX−XXX